Nonaqueous, Molecular Precursor Route to Hybrid Inorganic/Organic Zirconia−Silica Materials Containing Covalently Linked Organic Bridges

Richard L. Brutchey, Joshua E. Goldberger, Telly S. Koffas, and T. Don Tilley*

Department of Chemistry, University of California, Berkeley, Berkeley, California 94720-1460 and the Chemical Sciences Division, Lawrence Berkeley National Laboratory, 1 Cyclotron Road, Berkeley, California 94720

Received June 10, 2002. Revised Manuscript Received October 24, 2002

New hybrid inorganic/organic materials possessing zirconium in the inorganic framework have been synthesized. Co-thermolyses in sealed reactors (toluene, $AlCl_3$ catalyst, 155 °C) of $Zr[OSi(O^tBu)_3]_4$ in the presence of $(EtO)_3Si(CH_2)_nSi(OEt)_3$ ($n = 1, 2$) or $(EtO)_3Si(C_6H_4)_n$-$Si(OEt)_3$ ($n = 1, 2$; C_6H_4 = 1,4-phenylene) monomers rapidly yielded monolithic, transparent gels. The resulting xerogels were amorphous and exhibited high surface areas and high surface coverages of OH functionalities. Solid-state ^{29}Si and ^{13}C CP MAS NMR spectroscopies were used to establish the presence of intact, organic bridging groups and to verify the presence of unreacted ethoxy groups. Energy-dispersive X-ray spectroscopy was used to elucidate the elemental composition and distribution throughout the material, and atomic force microscopy was used to probe surface adhesive properties.

Introduction

Hybrid inorganic/organic materials have attracted considerable attention because of their unique chemical, mechanical, optical, and thermal properties that result from a combination of the inorganic and organic components.[1] Generally, hybrid materials can be divided into two classes: heterogeneous systems with phase-segregated inorganic and organic domains, and homogeneous systems with an intimate interpenetration of the organic and inorganic networks.[2] Included in this second class are bridged polysilsesquioxane hybrids, accessible by the sol−gel hydrolysis condensation of $(EtO)_3Si-R-Si(OEt)_3$ monomers (where R is a bridging hydrocarbon group) as developed by Shea, Loy and co-workers,[3] and by Corriu and co-workers.[4] These materials have found a variety of applications, for example in optics[5] and electronics,[6] and as coatings[7] and catalyst supports.[8]

Precise control over the solid-state structure of advanced materials remains a formidable task. One challenge in the development of hybrid materials is the incorporation of multiple elements into the inorganic oxide framework.[9] The sol−gel method is limited by the inherent difficulty in obtaining homogeneous materials because the metal and organosilane precursors hydrolyze at different rates, resulting in heterogeneity.[10] Our previous work over the past decade has focused on developing efficient routes to mixed-element oxide materials ($MO_2{\cdot}nSiO_2$) based on metal precursor complexes containing the $-OSi(O^tBu)_3$ ligand. Upon heating (100−150 °C), these molecular species cleanly eliminate

* To whom correspondence should be addressed. Phone: 510-642-8939. Fax: 510-642-8940. E-Mail: tilley@cchem.berkeley.edu.

(1) (a) Loy, D. A. *MRS Bull.* **2001**, *26*, 364. (b) Judeinstein, P.; Sanchez, C. *J. Mater. Chem.* **1996**, *6*, 511. (c) Lichtenhan, J. D. *Comments Inorg. Chem.* **1995**, *17*, 115. (d) Laine, R. M.; Zhang, C.; Sellinger, A.; Viculis, L. *Appl. Organomet. Chem.* **1998**, *12*, 715.
(2) Wen, J.; Wilkes, G. L. *Chem. Mater.* **1996**, *8*, 1667.
(3) (a) Shea, K. J.; Loy, D. A.; Webster, O. *J. Am. Chem. Soc.* **1992**, *114*, 6700. (b) Oviatt, H. W.; Shea, K. J.; Small, J. H. *Chem. Mater.* **1993**, *5*, 943. (c) Small, J. H.; Shea, K. J.; Loy, D. A. *J. Non-Cryst. Solids* **1993**, *160*, 234. (d) Loy, D. A.; Jamison, G. M.; Assink, R. A.; Zender, G.; Shea, K. J. *Polym. Mater. Sci. Eng.* **1993**, *70*, 373. (e) Loy, D. A.; Jamison, G. M.; Baugher, B. M.; Russick, E. M.; Assink, R. A.; Prabakar, S.; Shea, K. J. *J. Non-Cryst. Solids* **1995**, *186*, 44. (f) Loy, D. A.; Shea, K. J. *Chem. Rev.* **1995**, *95*, 1431. (g) Loy, D. A.; Jamison, G. M.; Baugher, B. M.; Myers, S. A.; Assink, R. A.; Shea, K. J. *Chem. Mater.* **1996**, *8*, 656. (h) Shea, K. J.; Loy, D. A. *MRS Bull.* **2001**, *26*, 402.
(4) (a) Corriu, R. J. P.; Moreau, J. J. E.; Thepot, P.; Man, M. W. C. *Chem. Mater.* **1992**, *4*, 1217. (b) Corriu, R. J. P.; Hesemann, P.; Lanneau, G. F. *Chem. Commun.* **1996**, 1845. (c) Cerveau, G.; Corriu, R. J. P.; Lepeytre, C. *Chem. Mater.* **1997**, *9*, 2561. (d) Cerveau, G.; Corriu, R. J. P.; Lepeytre, C.; Mutin, P. H. *J. Mater. Chem.* **1998**, *8*, 2707.
(5) (a) Oviatt, H. W.; Shea, K. J.; Kalluri, S.; Shi, Y.; Steier, W. H.; Dalton, L. R. *Chem. Mater.* **1995**, *7*, 493. (b) Xia, H.; Zhu, C.; Gan, F.; Chen, Y.; Yu, B.; Cai, R.; Huang, Z. *Fullerene Sci. Technol.* **1997**, *5*, 1621. (c) Corriu, R. J. P.; Moreau, J. J. E.; Thepot, P.; Man, M. W. C. *Chem. Mater.* **1994**, *6*, 640. (d) Bookbinder, D. C.; Wrighton, M. S. *J. Am. Chem. Soc.* **1980**, *102*, 5123. (e) Lebeau, B.; Brasselet, S.; Zyss, J.; Sanchez, C. *Chem. Mater.* **1997**, *9*, 1012.
(6) Lu, Y.; Fan, H.; Doke, N.; Loy, D. A.; Assink, R. A.; LaVan, D. A.; Brinker, C. J. *J. Am. Chem. Soc.* **2000**, *122*, 5258.
(7) Wang, B.; Wilkes, G. L. *J. Macromol. Sci., Pure Appl. Chem.* **1994**, *A31*, 249.
(8) (a) Linder, E.; Schneller, T.; Auer, F.; Mayer, H. A. *Angew. Chem., Int. Ed.* **1999**, *38*, 2155. (b) Inagaki, S.; Guan, S.; Fukushima, Y.; Ohsuna, T.; Teresaki, O. *J. Am. Chem. Soc.* **1999**, *121*, 9611. (c) Melde, B. J.; Holland, B. T.; Blanford, C. F.; Stein, A. *Chem. Mater.* **1999**, *11*, 3302. (d) Asefa, T.; MacLachlan, M. J.; Coombs, N.; Ozin, G. A. *Nature* **1999**, *402*, 867.
(9) Sanchez, S.; Ribot, F. *New J. Chem.* **1994**, *18*, 1007.
(10) (a) Wang, B.; Brennan, A. B.; Huang, H.; Wilkes, G. L. *J. Macromol. Sci., Chem.* **1990**, *A27*, 1447. (b) Wang, B.; Wilkes, G. L.; Smith, C. D.; McGrath, J. E. *Polym. Commun.* **1991**, *32*, 400. (c) Wang, B.; Wilkes, G. L. *J. Polym. Sci., Part A: Polym. Chem.* **1991**, *29*, 905. (d) Wang, B.; Wilkes, G. L.; Hedrick, J. C.; Liptak, S. C.; McGrath, J. E. *Macromolecules* **1991**, *24*, 3449. (e) Kickelbick, G.; Schubert, U. *J. Chem. Soc., Dalton Trans.* **1997**, 1301. (f) Lee, L.-H.; Chen, W.-C. *Chem. Mater.* **2001**, *13*, 1137. (g) Schubert, U.; Völkel, T.; Moszner, N. *Chem. Mater.* **2001**, *13*, 3811.

10.1021/cm020653+ CCC: $25.00
Published on Web 02/08/2003

isobutylene and water to give homogeneous, mixed-element oxide materials with well-defined stoichiometries.[11,12] For example, the thermal decomposition of $Zr[OSi(O^tBu)_3]_4$ occurs in solution (e.g., toluene) or in the solid-state under mild conditions (150 °C) to give a material ($ZrO_2 \cdot 4SiO_2$) in which all of the elements originate from a single molecular species (eq 1).[12]

$$Zr[OSi(O^tBu)_3]_4 \xrightarrow{\Delta} ZrO_2 \cdot 4SiO_2 + 12\ CH_2{=}CMe_2 + 6\ H_2O \quad (1)$$

The work herein describes the use of this nonaqueous, thermolytic molecular precursor approach in the preparation of relatively homogeneous hybrid inorganic/organic materials containing a transition element. The molecular precursor $Zr[OSi(O^tBu)_3]_4$ was used in the presence of $(EtO)_3Si{-}R{-}Si(OEt)_3$ compounds for the co-thermolytic synthesis of these hybrid materials. The resulting materials have potential applications as catalysts,[13] catalyst supports,[14] and structural materials with useful mechanical properties.[15]

Results and Discussion

Synthesis and Composition. The co-thermolytic syntheses (155 °C, $AlCl_3$ catalyst) of the hybrid network materials were carried out in toluene (eq 2). It is envisioned that the condensation of $Zr[OSi(O^tBu)_3]_4$ (**1**) with $(EtO)_3Si{-}R{-}Si(OEt)_3$ (**2**) requires the initial thermal decompositon of **1** to give isobutylene and reactive Si−OH species. The Si−OH groups then self-condense, or condense with Si−OEt groups from **2**, to form an inorganic/organic network material via the concomitant elimination of ethanol.

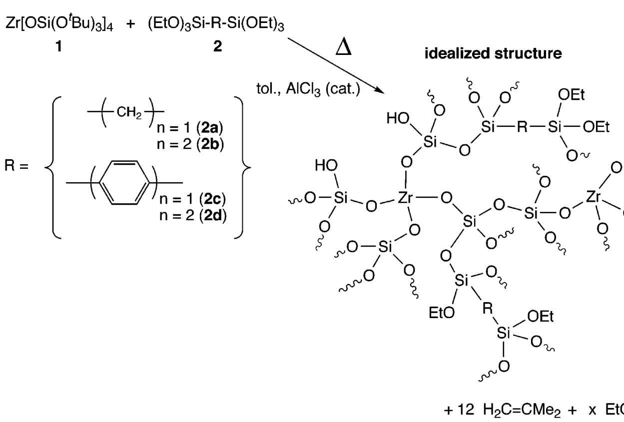

(2)

Branching and cross-linking occur until the network is extensive enough to produce a gel.[16]

Solution ^1H NMR spectroscopic studies demonstrated that heating benzene-d_6 solutions of **1** and **2a**−**d** (1:1 mol ratios) to 155 °C does not induce the thermolysis of **1** after 2 weeks, as suggested by the absence of isobutylene.[12c] Instead of gel formation, slow decomposition of **1** was observed by the formation of several broad resonances in the aliphatic region (0.93−1.33 ppm) of the ^1H NMR spectrum. The clean thermal decomposition of **1** at low temperatures appears to be inhibited by the presence of **2**, since it has been previously shown that **1** cleanly decomposes without the aid of a catalyst.[12c] However, the addition of a Lewis (e.g., $AlCl_3$) or Brønsted (e.g., HCl) acid is known to catalytically assist the thermal decomposition of molecular precursors containing the $-OSi(O^tBu)_3$ ligand.[11e,12a,b] Indeed, co-thermolyses of **1** and **2a**−**d** in benzene-d_6 in the presence of $AlCl_3$ (19 mol %) resulted in gel formation within minutes of heating (155 °C). The evolution of isobutylene from the complete thermal decomposition of **1** occurs immediately, with the formation of ethanol from the condensation of **2** occurring within ca. 10 min (as observed by ^1H NMR spectroscopy). After heating the reaction mixture for 24 h, **1** and **2** were completely consumed and incorporated into the material. Monomers **2a**−**d** are stable in the presence of $AlCl_3$ (155 °C, benzene-d_6), suggesting that the concurrent thermolytic decomposition of **1** is necessary for the condensation of **2** under these anhydrous conditions.

Bulk samples of the hybrid materials were obtained by combining monomers **1** and **2a**−**d** in toluene solutions containing a catalytic amount of $AlCl_3$. The solutions were sealed in a Parr reactor under an atmosphere of nitrogen, and heated to 155 °C for ca. 24 h. This preparation yielded monolithic, transparent gels with a slight yellow tint that are visually homogeneous in appearance. The gels were air-dried for 1 week, washed with pentane and toluene, and then air-dried again for 1 day. The final xerogels were then ground into fine powders and dried in vacuo at 120 °C for 12 h. Xerogel **$ZrSiCH_2$(1:1)** was formed from the 1:1 reaction of **1** and **2a**. Similarly, **$ZrSiCH_2$(1:4)** was formed from the 1:4 reaction of **1** and **2a**. Other xerogels were synthesized with 1:1 and 1:4 stoichiometric ratios of **1** and **2b**−**d**. For comparison, a material not containing bridging organic groups was synthesized from the 1:2 reaction of **1** and $Si(OEt)_4$ (TEOS). Properties for these materials are summarized in Table 1.

These materials contain significant quantities of unreacted ethoxy and hydroxy groups. This is indicated by the experimentally determined carbon contents for **$ZrSiCH_2$(1:1)**, **$ZrSiCH_2$(1:4)**, **$ZrSi(CH_2)_2$(1:1)**, and **$ZrSi(CH_2)_2$(1:4)** which were all 1.5−2.8 times the expected amount for a fully condensed material. Previously, Corriu and co-workers have reported that polysilses-

(11) (a) Terry, K. W.; Lugmair, C. G.; Gantzel, P. K.; Tilley, T. D. *Chem. Mater.* **1996**, *8*, 274. (b) Su, K.; Tilley, T. D. *Chem. Mater.* **1997**, *9*, 588. (c) Terry, K. W.; Su, K.; Tilley, T. D.; Rheingold, A. L. *Polyhedron* **1998**, *27*, 891. (d) Rulkens, R.; Male, J. L.; Terry, K. W.; Olthof, B.; Khodakov, A.; Bell, A. T.; Iglesia, E.; Tilley, T. D. *Chem. Mater.* **1999**, *11*, 2966. (e) Coles, M. P.; Lugmair, C. G.; Terry, K. W.; Tilley, T. D. *Chem. Mater.* **2000**, *12*, 122. (f) Kriesel, J. W.; Tilley, T. D. *J. Mater. Chem.* **2001**, *11*, 1081. (g) Fujdala, K. L.; Tilley, T. D. *Chem. Mater.* **2001**, *13*, 1817. (h) Lugmair, C. G.; Fujdala, K. L.; Tilley, T. D. *Chem. Mater.* **2002**, *14*, 888. (i) Fujdala, K. L.; Tilley, T. D. *Chem. Mater.* **2002**, *14*, 1376.

(12) (a) Terry, K. W.; Tilley, T. D. *Chem. Mater.* **1991**, *3*, 1001. (b) Terry, K. W.; Gantzel, P. K.; Tilley, T. D. *Chem. Mater.* **1992**, *4*, 1290. (c) Terry, K. W.; Lugmair, C. G.; Tilley, T. D. *J. Am. Chem. Soc.* **1997**, *119*, 9745. (d) Kriesel, J. W.; Sander, M. S.; Tilley, T. D. *Adv. Mater.* **2001**, *13*, 331.

(13) (a) Soled, S.; McVicker, G. B.; *Catal. Today* **1992**, *14*, 189. (b) Niwa, M.; Katada, N.; Murakami, Y. *J. Catal.* **1992**, *134*, 340. (c) Bosman, H. J. M.; Kruissink, E. C.; van der Spoel, J.; van der Brink, F. *J. Catal.* **1994**, *148*, 660. (d) Sohn, J. R.; Jang, H. J. *J. Mol. Catal.* **1991**, *64*, 349.

(14) (a) Miller, J. B.; Rankin, S. E.; Ko, E. I. *J. Catal.* **1994**, *184*, 673. (b) Miller, J. B.; Ko, E. I. *J. Catal.* **1996**, *159*, 58. (c) Kapoor, M. P.; Bhaumik, A.; Inagaki, S.; Kuraoka, K.; Yazawa, T. *J. Mater. Chem.* **2002**, *12*, 3078.

(15) Judeinstein, P.; Rault, J.; Alonso, B.; Sanchez, C. *J. Polym. Sci., Part B: Polym. Phys.* **2001**, *39*, 645.

(16) Brinker, C. J.; Scherer, G. W. *Sol*−*Gel Science: the Physics and Chemistry of Sol*−*Gel Processing*; Academic Press: Boston, 1990.

Table 1. Summary of Xerogel Properties

hybrid material[a]	organic spacer	surface area (m^2 g^{-1})	pore volume (cc g^{-1})	OH sites (nm^{-2})[b]	%C found (expected)[c]
$ZrSiCH_2$(1:1)	methylene	715	1.8	3.3 ± 0.2	7.1 (2.5)
$ZrSiCH_2$(1:4)	methylene	576	1.6	3.5 ± 0.2	11.8 (5.7)
$ZrSi(CH_2)_2$(1:1)	ethylene	707	0.68	2.9 ± 0.1	12.5 (4.8)
$ZrSi(CH_2)_2$(1:4)	ethylene	351	1.1	4.8 ± 0.3	18.9 (10.8)
$ZrSiC_6H_4$(1:1)	phenylene	745	0.89	4.4 ± 0.1	14.5 (13.3)
$ZrSiC_6H_4$(1:4)	phenylene	593	1.2	3.4 ± 0.2	29.41 (26.6)
$ZrSi(C_6H_4)_2$(1:1)	biphenylene	599	0.51	2.1 ± 0.1	18.38 (23.3)
ZrSi(1:2)	none	592	1.8	4.6 ± 0.2	4.32 (0)

[a] **ZrSiX(1:n)** is the nomenclature for materials where **X** is an organic spacer (**CH_2** = methylene, **$(CH_2)_2$** = ethylene, **C_6H_4** = phenylene, **$(C_6H_4)_2$** = biphenylene) and **n** is the stoichiometric ratio of **2** to **1**. [b] Errors are based on 2σ (95% confidence level) as determined from the integration of 10 ^{1}H NMR spectra monitored over 1 day. [c] Expected refers to a completely condensed material without residual ethoxy groups.

quioxane materials prepared by the sol−gel method possess uncondensed alkoxy groups.[4a] Extending the thermolysis time for **$ZrSi(CH_2)_2$(1:1)** and **$ZrSi(CH_2)_2$(1:4)** to several weeks did not affect the degree of condensation as determined by the amount of carbon found by combustion analysis. In addition, attempts to hydrolyze the ethoxy groups of the xerogels in acidic media (e.g., 2 M HCl (aq), 150° C) proved unsuccessful. Interestingly, the carbon contents of **$ZrSiC_6H_4$(1:1)** and **$ZrSiC_6H_4$(1:4)** are close to that expected for a fully condensed material. Surprisingly, however, the combustion analysis for **$ZrSi(C_6H_4)_2$(1:1)** revealed an unexpectedly low carbon content (18.4%) that was far below that expected for a fully condensed material (23.3%). We can only surmise that this material readily produces SiC during combustion, and thus retains some carbon during the analysis.[3a] Elemental analyses by inductively coupled plasma atomic emission spectroscopy (ICPAES) determined that the Si/Zr ratio ranged from 6.8:1 for **$ZrSi(CH_2)_2$(1:1)**, to 6.4:1 for **$ZrSiCH_2$(1:1)** and **$ZrSiC_6H_4$(1:1)**, to 5.5:1 for **$ZrSi(C_6H_4)_2$(1:1)**. The close agreement between these values and that expected (6:1 in each case) indicates that most of the silicon and zirconium from the monomers have been incorporated into the xerogels.

The conservation of the Si−R−Si linkage during the thermolytic process was confirmed by solid state ^{29}Si CP MAS NMR studies that provide connectivity information about the hybrid framework of the xerogels. The ^{29}Si CP MAS NMR spectra for **$ZrSiCH_2$(1:1)** and **$ZrSi(CH_2)_2$(1:1)** both reveal two broad resonances indicating the presence of trifunctional (T) and tetrafunctional (Q) silicon environments. The solid state ^{29}Si CP MAS NMR spectra for these two materials display broad resonances centered at ca. −61 ppm that span the chemical shift regions for T^1, T^2, and T^3 silicon environments.[3a,b,4a] In addition, both spectra contain a broad resonance centered at ca. −100 ppm, which spans the chemical shift ranges corresponding to Q^2, Q^3, and Q^4 silicon environments (Figure 1).[8d,12c] The T-silicon environments correspond to silicon atoms bound to the bridging R groups from **2**, and the Q-silicon environments correspond to ZrO-SiO_3 species derived from the molecular precursor **1**. The small fraction of observed Q^4 sites could arise from the separation of ZrO_2 domains or via Si−C bond cleavages leaving behind SiO_2. The solid state ^{29}Si CP MAS NMR spectrum for **$ZrSiC_6H_4$(1:1)** displays a broad T^2 resonance centered at −71 ppm, with distinct shoulders at −62 ppm (T^1) and −78 ppm (T^3). Another broad resonance centered at −101 ppm spans the chemical shift ranges for Q^2, Q^3, and Q^4 silicon environments (Figure 1). The spectrum obtained for **$ZrSi(C_6H_4)_2$(1:1)** contains similar chemical shifts for resonances of T (−61, −70, and −79 ppm) and Q (−101 ppm) silicon environments (Figure 1). The different chemical shifts for T resonances in such materials with aliphatic and arene bridges has been previously observed.[3a,b] Finally, **ZrSi(1:2)** exhibits only one broad resonance centered at −101 ppm corresponding to a Q silicon environment, as expected. These results are summarized in Table 2.

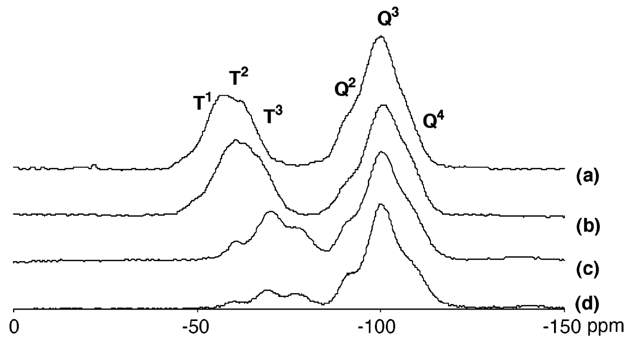

Figure 1. ^{29}Si CP MAS NMR spectra of **$ZrSi(CH_2)_2$(1:1)** (a), **$ZrSiCH_2$(1:1)** (b), **$ZrSiC_6H_4$(1:1)** (c), and **$ZrSi(C_6H_4)_2$(1:1)** (d) showing T^1, T^2, and T^3 resonances from bridging silicon atoms and Q^2 and Q^3 resonances from inorganic framework silicon atoms.

Table 2. ^{29}Si CP MAS NMR Data

xerogel	T resonances (ppm)	Q resonances (ppm)
$ZrSiCH_2$(1:1)	−60 (br[a])	−101 (br)
$ZrSi(CH_2)_2$(1:1)	−61 (br)	−102 (br)
$ZrSiC_6H_4$(1:1)	−62, −71, −78	−101 (br)
$ZrSi(C_6H_4)_2$(1:1)	−61, −70, −79	−101 (br)
ZrSi(1:2)	N/A	−101 (br)

[a] br = broad resonance.

To verify retention of the organic bridges and corroborate the presence of unreacted ethoxy groups in these materials, they were examined by ^{13}C CP MAS NMR spectroscopy. Each of the xerogels **$ZrSiCH_2$(1:1)**, **$ZrSi(CH_2)_2$(1:1)**, **$ZrSiC_6H_4$(1:1)**, and **$ZrSi(C_6H_4)_2$(1:1)** exhibit ^{13}C NMR resonances for unreacted ethoxy groups (Table 3). The methyl and methylene resonances from residual ethoxy groups lie between 15.8 and 16.2 and 58.0 and 58.7 ppm, respectively. ^{13}C NMR resonances are also observed for the bridging organic groups. The bridging methylene carbon in **$ZrSiCH_2$(1:1)** is observed as a broad resonance at −2.1 ppm, and the bridging methylene carbons in **$ZrSi(CH_2)_2$(1:1)** are observed as a broad resonance at 3.8 ppm. The bridging phenylene carbons in **$ZrSiC_6H_4$(1:1)** are observed at 126.4 and 132.8 ppm. Also, three of the four expected

Table 3. ^{13}C CP MAS NMR Data

xerogels	$^{13}C(Si-R-Si)$ (ppm)	$^{13}C(-OCH_2)$ (ppm)	$^{13}C(CH_3)$ (ppm)
$ZrSiCH_2$(1:1)	−2.1 (br[a])	58.0	15.8
$ZrSi(CH_2)_2$(1:1)	3.8 (br)	58.7	16.2
$ZrSiC_6H_4$(1:1)	132.8, 126.4	58.7	15.8
$ZrSi(C_6H_4)_2$(1:1)	142.0, 133.5, 126.8	58.6	15.8

[a] br = broad resonance.

phenylene carbons in **$ZrSi(C_6H_4)_2$(1:1)** are observed at 126.8, 133.5, and 142.0 ppm. The fourth expected resonance is probably obscured by the other peaks. In addition to the expected $-OCH_2CH_3$ and Si−R−Si resonances, an additional, minor resonance at ca. 29 ppm is observed for **$ZrSiCH_2$(1:1)**, **$ZrSiC_6H_4$(1:1)**, and **$ZrSi(C_6H_4)_2$(1:1)**. In the case of **$ZrSi(CH_2)_2$(1:1)** this resonance is quite strong. We attribute this peak to alcohol trapped in the materials (i.e., *tert*-butyl alcohol from the thermal decomposition of **1**[12c]).

FTIR spectra of dried xerogels containing methylene and ethylene bridges exhibit the appropriate alkyl C−H stretching vibration bands at ca. 2930−2960 cm^{-1}. The strong, broad peak observed for Si−O−Si at ca. 1070 cm^{-1} obscures bands associated with Si−C modes. The FTIR spectra of **$ZrSiC_6H_4$(1:1)** display characteristic aromatic C−H stretching bands at 3065 cm^{-1} and what is likely a Si−Ph band at 1152 cm^{-1}. Similar bands at 3035 cm^{-1} (for C−H aromatic stretches) and 1136 cm^{-1} (for Si−Ph) are observed for **$ZrSi(C_6H_4)_2$(1:1)**. As expected, calcination of each as-prepared material to 500 °C under a flow of oxygen for 2 h removes most of the organic material from the xerogels as determined by combustion analysis and FTIR spectroscopy. Additionally, by diffuse reflectance UV−vis spectroscopy, a strong absorption at 278 nm is observed for **$ZrSiC_6H_4$(1:1)** and one at 287 nm is present for **$ZrSi(C_6H_4)_2$(1:1)**. These absorptions correspond to the $\pi \rightarrow \pi^*$ transition for the aromatic systems, and correlate with the λ_{max} values (276 and 288 nm, respectively) observed for the respective monomers **2c** and **2d** (in pentane solution).

Physical Properties. The hybrid materials are amorphous in nature as indicated by powder X-ray diffraction (PXRD). Amorphous $n ZrO_2 \cdot m SiO_2$ materials, from the cohydrolysis of $Zr(OR)_4$ and $Si(OR')_4$ compounds, typically exhibit crystallization of the ZrO_2 between 800 and 1100 °C.[17] This is often indicative of a homogeneously mixed $n ZrO_2 \cdot m SiO_2$ material, since high temperatures are needed for the phase separation and grain growth of crystalline ZrO_2.[12d,18] Only after calcination of **$ZrSi(CH_2)_2$(1:1)** to 1000 °C under oxygen over 4 h were small domains of monoclinic-ZrO_2 observed as very broad peaks in the PXRD pattern.[12c] This suggests that the few Q^4 silicon environments observed by ^{29}Si CP MAS NMR spectroscopy are not a result of ZrO_2 phase separation, but arise via some degree of Si−C bond cleavage. It is important to note, however, that by ^{13}C CP MAS NMR spectroscopy the organic bridges appear to remain intact.

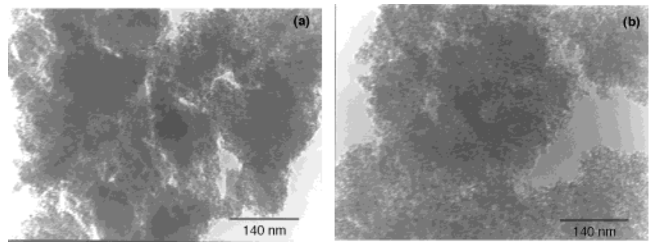

Figure 2. TEM micrographs of **$ZrSi(CH_2)_2$(1:1)** (a) and **$ZrSiCH_2$(1:1)** (b).

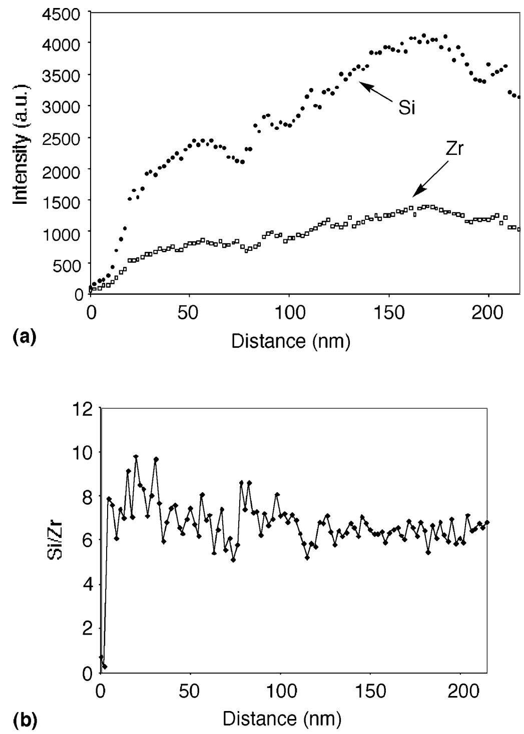

Figure 3. (a) EDS profile of **$ZrSiCH_2$(1:1)** performed using a 1.5-nm probe at 2.2-nm intervals (30 s/pt). Points shown as filled circles and open boxes correspond to Si and Zr, respectively. (b) The ratio of Si/Zr at each point along the profile for **$ZrSiCH_2$(1:1)**.

Transmission electron microscopy (TEM) studies of the as-synthesized hybrid materials **$ZrSiCH_2$(1:1)** and **$ZrSi(CH_2)_2$(1:1)** revealed aggregates of fine granules with a wide range of particle sizes (Figure 2). To probe the homogeneity of the materials, energy-dispersive X-ray spectroscopy (EDS) was used to assess the stoichiometry of the inorganic elements in **$ZrSiCH_2$(1:1)**. EDS profiles taken from large (ca. 600 nm) areas confirmed that the Si/Zr ratio of 5.8(±0.6):1 is close to that of the expected Si/Zr ratio of 6.4:1 (from ICPAES). In addition, local EDS spectroscopy at high spacial resolution was used to assess the distribution of silicon and zirconium. The EDS profile (Figure 3) of **$ZrSiCH_2$(1:1)** illustrates the relative amount of Si and Zr along a 220-nm piece of sample (ca. 2.2 nm acquisition intervals), using a 1.5-nm beam spot size. The intensities of the points for both Si and Zr increase over the sampling length as a result of an increase in the

(17) (a) Garvie, R. C. *J. Phys. Chem.* **1978**, *82*, 218. (b) Jansen, M.; Guenther, E. *Chem. Mater.* **1995**, *7*, 2110. (c) Andrianainarivelo, M.; Corriu, R.; Leclerq, D.; Mutin, P. H.; Vioux, A. *J. Mater. Chem.* **1996**, *6*, 1665. (d) Li, X.; Johnson, P. F. In *Better Ceramics Through Chemistry*; Zelinski, B. J. J., Brinker, C. J., Clark, D. E.; Ulrich, D. R., Eds.; Mater. Res. Soc. Symp. Proc. Vol. 180; Materials Research Society: Pittsburgh, PA, 1990; p 355.

(18) (a) Osendi, M. I.; Moya, J. S.; Serna, C. J.; Soria, J. *J. Am. Ceram. Soc.* **1985**, *68*, 135. (b) Garvie, R. C. *J. Phys. Chem.* **1965**, *69*, 1238. (c) Nagarajan, V. S.; Rao, K. J. *J. Mater. Sci.* **1989**, *24*, 2140. (d) Lange, F. F. *J. Mater. Sci.* **1982**, *17*, 235. (e) Heuer, A. H.; Claussen, N.; Kriven, W. M.; Rühle, M. *J. Am. Ceram. Soc.* **1982**, *65*, 642. (f) Skandan, G.; Hahn, H.; Roddy, M.; Cannon, W. R. *J. Am. Ceram. Soc.* **1994**, *77*, 1706.

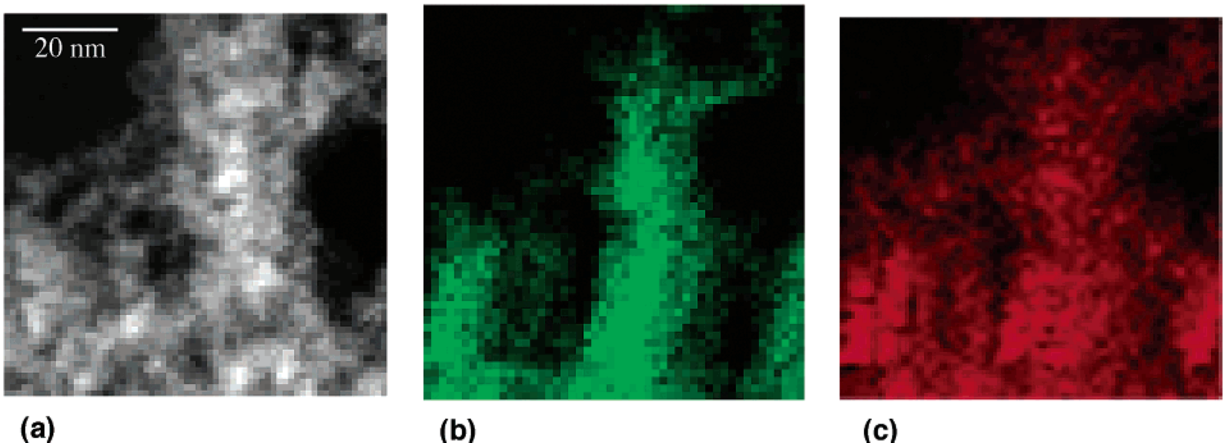

Figure 4. Selected area TEM micrograph of **$ZrSiCH_2$(1:1)** (a), and EDS elemental maps of Si K (b) and Zr L peaks (c). Pixel size is 1.6 nm. Regions with higher Si and Zr concentrations in (b) and (c), respectively, appear bright.

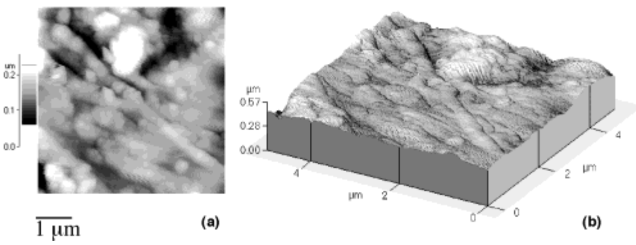

Figure 5. AFM top view (a), and topographical view (b), of **$ZrSiCH_2$(1:1)**.

thickness of the sample. Figure 3b shows the Si/Zr ratio over the 220 nm region of **$ZrSiCH_2$(1:1)**. The Si/Zr ratios range from approximately 10:1 to 5:1, with the average being ca. 6.7:1. Also, EDS profiles taken from 10 random local areas (1.2-nm beam spot size) gave a Si/Zr ratio of 6.3(±0.6):1. This confirms that the ratio of inorganic elements is relatively constant for **$ZrSiCH_2$(1:1)**, even on the scale of 1.2−1.5 nm, and the elements are fairly homogeneous in their dispersion throughout the material. Figure 4 qualitatively illustrates the EDS elemental maps of silicon and zirconium for **$ZrSiCH_2$(1:1)**. It is evident from the elemental maps that the two elements are reasonably well-mixed in the bulk of the material.

Atomic force microscopy (AFM) was used to study the topographical and surface adhesive properties of the hybrid materials and a purely inorganic sample (ZrO_2·$4SiO_2$), for comparison. The topography of **$ZrSiCH_2$(1:1)**, as observed by AFM, is shown in Figure 5. The root-mean-square (rms) roughness for this material is 37.0 nm. This is comparable to the rms roughness for **$ZrSi(CH_2)_2$(1:1)** and ZrO_2·$4SiO_2$ which are 25.6 and 31.4 nm, respectively. The morphological information obtained by scanning electron microscopy (SEM) (Figure 6) supports the topographical information obtained by AFM.

The surface properties were probed by examining adhesive forces between the silicon nitride tip (force constant $k = 1.0$ N m^{-1}; radius of curvature = ∼50 nm) and **$ZrSiCH_2$(1:1)**, **$ZrSi(CH_2)_2$(1:1)**, and ZrO_2·$4SiO_2$ under ambient conditions (25 °C, 35% relative humidity). A uniformly high adhesion was observed for ZrO_2·$4SiO_2$ with an average adhesive force of 89.0 ± 2.9 nN. Such high adhesion may indicate the presence of a surface water layer as capillary forces are usually on the order of 100 nN.[19] This is consistent with the hydrophilic nature of the surface of this oxide. A relatively uniform low adhesion was observed for **$ZrSiCH_2$(1:1)**, with an average adhesive force of 19.8 ± 0.5 nN. Approximately 15% of the area probed exhibited a lower adhesion of 8.9 ± 1.0 nN. Similarly, **$ZrSi(CH_2)_2$(1:1)** had low adhesion with an average adhesive force of 17.2 ± 1.1 nN. For this sample, however, a larger percentage of the area probed (ca. 35%) exhibited lower adhesion with an average adhesive force of 9.3 ± 1.1 nN. The surface adhesion properties of the hybrid materials are substantially different from those of the purely inorganic ZrO_2·$4SiO_2$ material, suggesting that the surface of the hybrid materials does not contain inorganic domains similar to those of ZrO_2·$4SiO_2$.[20] The lower adhesion observed for the hybrid materials is likely a result of the more organic-rich, hydrophobic surface of these materials. It is possible that surface domains that are particularly organic-rich in character exist at the areas of very low adhesion (i.e., ca. 9 nN). The radius of curvature (∼50 nm) of the silicon nitride tip limits measuring the domain size of these areas, however, below this resolution.

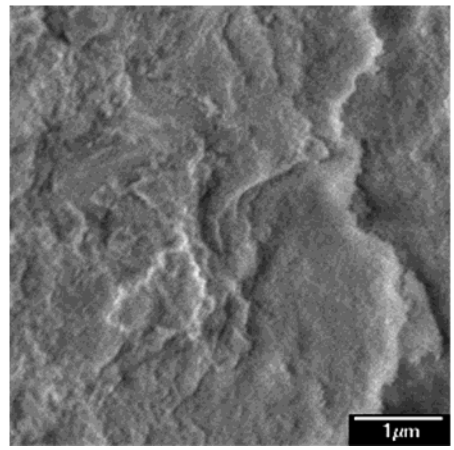

Figure 6. SEM micrograph of **$ZrSiCH_2$(1:1)**.

Nitrogen porosimetry was used to evaluate the pore structures and surface areas of the materials. The

(19) (a) Xiao, X.; Qian, L. *Langmuir* **2000**, *16*, 8153. (b) Binggeli, M.; Mate, C. M. *Appl. Phys. Lett.* **1994**, *65*, 415.

(20) (a) Schiavon, G.; Kuchler, J. G.; Corain, B.; Hiller, W. *Adv. Mater.* **2001**, *13*, 310. (b) Gao, Y.; Choudhury, N. R.; Dutta, N.; Matisons, J.; Reading, M.; Delmotte, L. *Chem. Mater.* **2001**, *13*, 3644.

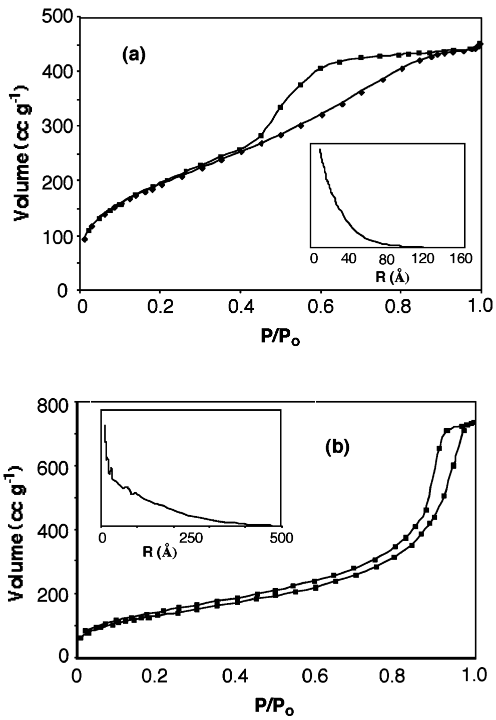

Figure 7. Nitrogen adsorption−desorption isotherms for **ZrSi(CH$_2$)$_2$(1:1)** (a) and **ZrSi(CH$_2$)$_2$(1:4)** (b). Adsorption pore size distributions are shown as insets.

adsorption−desorption data correspond to type IV isotherms,[21] suggesting some mesoporosity, however much of the porosity appears to result from micropores with radii <20 Å (Figure 7). A steep rise in adsorbed volume at relative pressure (P/P_o) > 0.8 indicates textural mesoporosity.[22] Thus, mesoporosity in the case of **ZrSi(CH$_2$)$_2$(1:4)**, for example, most likely arises from voids between the particles (Figure 7b). The hybrid materials were found to have high BET surface areas;[23] the xerogels obtained from **1** and **2** had surface areas ranging from 351 m^2 g^{-1} for **ZrSi(CH$_2$)$_2$(1:4)** to 745 m^2 g^{-1} for **ZrSiC$_6$H$_4$(1:1)** (Table 1). With an increase in the **2**/**1** molar ratio (to 4:1), the surface areas of the xerogels decreased in all cases by at least 20%. This suggests that a high concentration of molecular precursor **1** is necessary to obtain high-surface-area materials under these conditions. Calcination of **ZrSi(CH$_2$)$_2$(1:1)** to 500 °C under a flow of oxygen for 3 h resulted in a decrease in surface area to 490 m^2 g^{-1}, possibly as a result of collapse of the network upon loss of organic material. For comparison, the hybrid materials reported here have BET surface areas that are comparable to those for ZrO_2·4SiO_2 materials synthesized from the thermal decomposition of **1** under identical conditions (ca. 600 m^2 g^{-1}). Also, the co-thermolysis of TEOS and **1** afforded xerogel **ZrSi(1:2)** with a comparable surface area (592 m^2 g^{-1}).

The concentration of Brønsted acid sites (OH) was determined by quantifying the amount of toluene evolved after reaction of the xerogels with Mg(CH$_2$Ph)$_2$·2THF.[11h,24] As shown in Table 1, these materials possess high concentrations of Brønsted acid sites. For comparison, similar measurements performed on ZrO_2·4SiO_2 (surface area = 600 m^2 g^{-1}) obtained from the thermolysis of **1** in the presence of an $AlCl_3$ catalyst gave an OH coverage of 5.7 nm^{-2}.

Thermal Stability. Thermogravimetric analyses (TGA) of the hybrid materials demonstrated degradation of the materials beginning at ca. 250 °C under a flow of oxygen. The mass loss occurring below 200 °C (7−8%) is attributed to the thermal desorption of water[25] adsorbed during handling of the materials (in air) prior to the measurement. The weight loss between 200 and 1000 °C is attributed to the loss of framework organic fragments and residual ethoxy groups in the materials. The mass loss for each material was consistent with the carbon and hydrogen contents found by combustion analysis. Analysis of these materials by DSC revealed the occurrence of exothermic transitions between 270 and 380 °C. These transitions appear to be associated with combustion of the organic fragments and loss of mass in the materials. However, distinct exothermic transitions for losses of ethoxy groups and loss of organic bridges were not observed.

Conclusion

Hybrid zirconia−silica materials containing covalently linked organic bridges have been prepared by a new method involving a modification of the thermolytic molecular precursor approach.[11,12] The transformations involving **1** and **2** provide a convenient synthetic pathway to hybrid inorganic/organic materials containing a transition metal and a series of organic spacers. Gel formation occurs rapidly (ca. 10 min) in nonpolar media and affords high-surface-area xerogels upon drying. The as-synthesized materials are highly functionalized with surface OH groups (up to 4.8 sites nm^{-2}). In addition, the surface adhesive properties of the hybrid materials indicate that the surfaces are organic-rich and hydrophobic in nature. Also, solid state ^{29}Si and ^{13}C CP MAS NMR spectroscopies indicate that the Si−R−Si linkages from precursors **2** remain intact in the final hybrid materials. EDS analysis of **ZrSiCH$_2$(1:1)** indicates that silicon and zirconium are fairly well-mixed in the inorganic framework of this material. This method offers the opportunity to synthesize a wide variety of hybrid materials that combine transition metals with diverse organic spacers.

Experimental Procedures

General Procedures. All manipulations were conducted under a nitrogen atmosphere using standard Schlenk techniques or in a Vacuum Atmospheres drybox, unless otherwise noted. Dry, oxygen-free solvents were used throughout. Benzene-d_6 was purified and dried by vacuum distillation from sodium/potassium alloy.

Monomer **2a** was purchased from Gelest, Inc. and used without further purification. Monomer **2b** was purchased from Gelest, Inc. and distilled prior to use. Monomers **2c** and **2d** were prepared by literature methods.[3a] Anhydrous $AlCl_3$ was purchased from Aldrich (99.99% purity) and sublimed prior to use. The compounds HOSi(O^{t}Bu)$_3$[26] and Zr(NMe$_2$)$_4$[27] were

(21) Sing, K. S. W. *Pure Appl. Chem.* **1985**, *57*, 603.
(22) Tanev, P. T.; Pinnavaia, T. J. *Chem. Mater.* **1996**, *8*, 2068.
(23) Gregg, S. J.; Sing, K. S. W. *Adsorption, Surface Area, and Porosity*, 2nd ed.; Academic Press: London, 1982.
(24) Fujdala, K. L.; Tilley, T. D. *J. Am. Chem. Soc.* **2001**, *123*, 10133.
(25) Jaroniec, C. P.; Kruk, M.; Jaroniec, M.; Sayari, A. *J. Phys. Chem. B* **1998**, *102*, 5503.
(26) Abe, Y.; Kijima, I. *Bull. Chem. Soc. Jpn.* **1969**, *42*, 1118.

prepared as reported in the literature. The compound Zr[OSi-(O^{t}Bu)$_3$]$_4$ (**1**) was prepared by a modified procedure,[12c] using Zr(NMe$_2$)$_4$ instead of Zr(NEt$_2$)$_4$, in a yield of 72%.

Gelation of 1 and 2a in toluene [ZrSiCH$_2$(1:1)]. The preparations of all gels were carried out according to the following general procedure. A toluene solution (6.0 mL) of **1** (0.600 g, 0.524 mmol), **2a** (0.191 g, 0.545 mmol), and AlCl$_3$ (0.009 g, 0.070 mmol) was sealed in a 20-mL Parr reactor in a drybox. The reactor was placed in a preheated oven (155 °C) for 26 h. The wet gel was removed and air-dried for 7 days to form a xerogel. The xerogel was rinsed with pentane (2 × 5 mL) and toluene (2 × 5 mL) and was allowed to air-dry for 1 day. The off-white xerogel was ground into a fine powder and dried in vacuo for 12 h at 120 °C to yield 0.216 g of material. Repeated synthesis of **ZrSiCH$_2$(1:1)** yielded a material with similar carbon and hydrogen content, and with the same surface area (within experimental error).

Characterization. Solution ^{1}H NMR spectra were recorded at 400 MHz using a Bruker AM-400 spectrometer and were referenced internally to the residual solvent proton signal relative to tetramethylsilane. ^{13}C CP MAS NMR data were collected on a CMX400 Infinity spectrometer based on a 9.4 T magnet, with a frequency of 100.615 MHz, a spectrum width of 100 kHz, 90° pulse length of 8 μs, contact time of 2−3 ms, and a pulse delay time of 5 s. Tetramethylsilane was used as an external chemical shift reference and the samples were spun at 3.2−3.5 kHz. ^{29}Si CP MAS NMR data were collected with a frequency of 79.4867 MHz, spectrum width of 50 kHz, 90° pulse length of 8 μs, contact time of 5 ms, and pulse delay of 5 s. Tetramethylsilane was used as an external chemical shift reference and the samples were spun at 3.0−3.5 kHz. Infrared spectra were recorded as KBr disks using a Mattson FTIR spectrometer. Elemental analyses were performed by the College of Chemistry microanalytical laboratory at the University of California, Berkeley or at Mikro Analytisches Labor Pascher. PXRD experiments were performed on a Siemens D5000 X-ray diffractometer using Cu Kα radiation. Transmission electron microscopy was carried out on a JEOL 200CX transmission electron microscope operating at 200 kV. Samples for energy-dispersive spectroscopy (EDS) were studied on a Phillips CM-200 transmission electron microscope operating at 200 kV. EDS spectra were taken on a Gatan detector connected to the electron microscope. Samples for TEM studies were prepared by depositing a pentane suspension of the finely ground xerogels onto carbon-coated copper grids obtained from Ted Pella, Inc. Field emission scanning electron microscopy (FESEM) was carried out on a JEOL JSM-634OF electron microscope operating at 20 kV. Atomic force microscopy (AFM) was carried out on a Park Scientific Instruments Autoprobe M5 AFM. A Thermal Microscopes pyramidal, silicon nitride cantilever probe was used, whose force constant is 1.0 N m^{-1} and radius of curvature is ∼50 nm. Samples for AFM and SEM studies were prepared by making a neat pellet of the xerogels using a hydraulic press. Nitrogen absorption isotherms were measured on a Quantachrome Autosorb 1 surface area analyzer, and samples were outgassed at 120 °C for at least 3 h prior to measurement. Thermal analyses were performed on a TA Instruments SDT 2960 Integrated TGA/DSC analyzer with a heating rate of 10 °C min^{-1} under a flow of oxygen. Calcinations were performed using a Lindberg 1200 °C three-zone tube furnace with a heating rate of 10 °C min^{-1} under a flow of oxygen and the temperature was held constant at 700 °C for 3 h.

Acknowledgment. This work was supported by the Director, Office of Energy Research, Office of Basic Energy Sciences, Chemical Sciences Division, of the U.S. Department of Energy under Contract DE-AC03-76SF00098. R.L.B. thanks the National Science Foundation for support with a NSF Graduate Fellowship. We thank B. L. Phillips and P. Yu at the University of California, Davis, for the CP MAS NMR spectra and A. M. Stacy at the University of California, Berkeley for the use of instrumentation (PXRD, DRUV-vis). We are grateful to C. Nelson and D. Ah Tye for technical assistance with electron microscopy and the National Center for Electron Microscopy for use of their instruments.

Supporting Information Available: A representative TGA trace, ^{13}C CP MAS NMR spectrum, FTIR spectrum, and DRUV−vis spectrum are presented. This material is available free of charge via the Internet at http://pubs.acs.org.

CM020653+

(27) Diamond, G. M.; Rodewald, S.; Jordon, R. F. *Organometallics* **1995**, *14*, 5.